Front. Optoelectron. 2020, 13(3): 272–281
https://doi.org/10.1007/s12200-020-1031-1

RESEARCH ARTICLE

Surfactant-assisted doctor-blading-printed $FAPbBr_3$ films for efficient semitransparent perovskite solar cells

Hangkai YING[1], Yifan LIU[1], Yuxi DOU[1], Jibo ZHANG[1], Zhenli WU[1], Qi ZHANG[2,3], Yi-Bing CHENG[1,4], Jie ZHONG (✉)[1]

1 State Key Laboratory of Advanced Technology for Materials Synthesis and Processing, Wuhan University of Technology, Wuhan 430070, China
2 School of Materials Science and Engineering, Wuhan University of Technology, Wuhan 430070, China
3 School of Aerospace, Transport and Manufacturing, Cranfield University, Cranfield, Bedfordshire, MK43 0AL, UK
4 Department of Materials Science and Engineering, Monash University, VIC 3800, Australia

© Higher Education Press 2020

Abstract Organic–inorganic hybrid perovskite solar cells have generated wide interest due to the rapid development of their photovoltaic conversion efficiencies. However, the majority of the reported devices have been fabricated via spin coating with a device area of < 1 cm^2. In this study, we fabricated a wide-bandgap formamidinium lead bromide ($FAPbBr_3$) film using a cost-effective, high-yielding doctor-blade-coating process. The effects of different surfactants, such as l-α-phosphatidylcholine, polyoxyethylene sorbitan monooleate, sodium lauryl sulfonate, and hexadecyl trimethyl ammonium bromide, were studied during the printing process. Accompanying the optimization of the blading temperature, crystal sizes of over 10 μm and large-area perovskite films of 5 cm × 5 cm were obtained using this method. The printed $FAPbBr_3$ solar cells exhibited a short-circuit current density of 8.22 mA/cm^2, an open-circuit voltage of 1.175 V, and an efficiency of 7.29%. Subsequently, we replaced the gold with silver nanowires as the top electrode to prepare a semitransparent perovskite solar cell with an average transmittance (400–800 nm) of 25.42%, achieving a high-power efficiency of 5.11%. This study demonstrates efficient doctor-blading printing for preparing large-area $FAPbBr_3$ films that possess high potential for applications in building integrated photovoltaics.

Keywords semitransparent, printing, perovskite solar cell (PSC), doctor blading, wide bandgap

1 Introduction

Semitransparent solar cells are an ideal choice for building integrated photovoltaics, which can be used as electricity-generating facades, roofs, and windows [1,2]. Moreover, such devices can also be used in electric cars and tandem solar cells [3]. Organic–inorganic hybrid perovskite solar cells (PSCs) have generated wide interest since 2009 due to their unprecedented high efficiency and potential economic advantages as a low-cost photovoltaic technology [4–6]. There are many amazing optoelectronic properties of perovskite materials, such as a high carrier mobility, a long charge diffusion length, and a high absorption coefficient, which promise high power conversion efficiencies (PCEs) for PSCs [7] of more than 25.0% [8]. By regulating the thickness of the perovskite layers and/or using wide-bandgap perovskite materials and transparent electrodes, semitransparent perovskite solar cells (ST-PSCs) can easily be prepared for future potential applications due to their solution-compatible processing. Wide-bandgap perovskite materials, such as formamidinium lead bromide ($FAPbBr_3$), with a bandgap of ~2.23 eV and absorption spectra in the range of 300–550 nm, are especially appropriate for ST-PSCs with low temperature (150°C) processability compared to their inorganic counterpart $CsPbBr_3$. Currently, the highest performance of a $FAPbBr_3$ solar cell has reached 10.6% using a spin-coating method for the device preparation [9].

With the goal of the abovementioned applications, it would be beneficial to prepare large-scale PSCs under ambient conditions to keep production costs as low as possible. The development of high-yielding printing methods is crucial for rapid and cost-effective production. However, most of the reported devices have been fabricated via spin coating with active device area of < 1

Received May 1, 2020; accepted June 10, 2020

E-mail: jie.zhong@whut.edu.cn

cm^2. Therefore, an alternative route for the large-scale output of perovskite film is preferred. In the past few years, large-scale printing processes have been reported, such as spray coating [10], soft-cover deposition [11], doctor-blade coating [12–14], and slot-die coating [15,16]. Due to the simplicity of doctor-blade coating, this method has successfully drawn the attention of researchers and has become one of the most widely used methods in laboratories. Meanwhile, blade coating is a printing method that is highly compatible with high-yielding roll-to-roll coating [17,18]. In contrast to spin coating, there is no doubt that doctor-blade coating is a cost-effective and simple process that has a great advantage in utilizing the rheological characteristics and drying kinetics of precursor solutions [19]. In 2015, blade coating was used in PSC fabrication for the first time achieving an ~15.0% PCE [18]; this efficiency then very quickly increased to 19.0% for small-area devices [14,20]. Due to the increased difficulty of film morphology control during blade coating [21], it is generally more difficult to obtain high-quality films with blade coating than with spin coating [5]. How to control the uniformity of bladed-coated films is the main obstacle to obtaining large-area devices with high performance.

In this study, we demonstrated a doctor-blading process to fabricate high-quality perovskite $FAPbBr_3$ thin films taking advantage of the excellent solution processability of $FAPbBr_3$ perovskite and its high-performance humidity stability [22]. We studied the effects of the addition of surfactants to the $FAPbBr_3$ perovskite precursor for the doctor-blading process, which significantly enhanced the quality of the film on the substrate. For planar heterojunction PSCs with a regular classical architecture of fluorine-doped tin oxide-coated glass (FTO)\$TiO_2$\$FAPbBr_3$\Spiro-OMeTAD\Au, the PCEs of the devices prepared via blade coating were up to 7.29%. For the semitransparent perovskite devices, we selected silver nanowires (AgNWs) as the electrodes to replace the opaque gold metal. The PCEs of the wide-bandgap ST-PSCs fabricated via blade coating were up to 5.11%.

2 Experimental

2.1 Materials

Titanium chloride ($TiCl_4$, 99.9%) was purchased from Shanghai HUSHI Laboratory Equipment Co., Ltd., China; formamidinium bromine (FABr, 99.99%) and lead bromide ($PbBr_2$, 99.99%) were purchased from Xi'an p-OLED Photoelectric Technology Co., Ltd., China; Spiro-OMeTAD was purchased from Shenzhen Feiming Science and Technology Co., Ltd., China; and all of the solvents were purchased from Aladdin without further purification.

2.2 Preparation of TiO_2 films

The titanium dioxide (TiO_2) films were prepared according to a previously reported procedure [23]. In brief, in an ice and water bath environment, 112 mL of $TiCl_4$ was slowly dissolved in 388 mL of deionized water. The TiO_2 precursor solution was stirred for 5 h at room temperature in air when the solution became pellucid. The TiO_2 film was formed via chemical bath deposition. Cleaned FTO glass was covered by a 100-mL mixed solution of the TiO_2 precursor solution and deionized water and placed in an oven at 70°C for 40 min; the FTO glass was then washed and the process repeated until the film was finally annealed at 450°C for 30 min. The resulting TiO_2 electron transport layer was approximately 20-nm thick.

2.3 Device fabrication

First, the FTO glass was etched using a femtosecond laser to form the designed patterns. Then, ultrasonic cleaning was performed using deionized water and ethyl alcohol for 20 min. The mixed perovskite precursor solution was prepared by dissolving metal lead salts ($PbBr_2$) and organic cations (FABr) into a mixture solvent of N,N-dimethylformamide (DMF)/dimethyl sulfoxide (DMSO) (4:1, by volume) forming a 0.7 mol/L solution of $FAPbBr_3$. The formamidinium lead bromide ($FAPbBr_3$) perovskite thin film was fabricated via blade coating on top of the electron transport layer under ambient conditions. During deposition, the substrate was heated and then a 10–20 μL perovskite solution was dropped onto the substrate followed by blading at a constant speed of 200 cm/min. The resulting films were sequentially annealed at 150°C for 20 min. The hole transport layer was spun on the perovskite films at 3000 r/min for 30 s using a chlorobenzene (CBZ) solution, which was prepared by dissolving 73 mg of Spiro-OMeTAD into 1 mL of CBZ doped by 30 μL of 4-tert-butylpyridine, 18 μL of 520 mg/mL lithium bis(trifluoromethanesulfonyl)imide (Li-TFSI), and 29 μL of 300 mg/mL FK209. Finally, a 70-nm-thick Au electrode was deposited via thermal evaporation. For the ST-PSCs, the Au electrode was replaced by spray-prepared silver nanowires.

2.4 Characterization

Scanning electron microscopy (SEM, Phenom Pro) was used to characterize the morphologies of the different perovskite films. X-ray diffraction (XRD, Bruker AXS D8 Advance) was used to measure the XRD spectra of the different perovskite films. The optical properties of the perovskite films were measured using a UV/vis/NIR spectrophotometer (PerkinElmer Lambda 750s). Current density–voltage (*J–V*) curves were measured under AM

1.5 G one sun illumination (100 mW/cm^2) using a solar simulator (Oriel 94023 A, 300 W) and a Keithley 2400 source meter. The external quantum efficiency (EQE) spectra were all calibrated using crystalline silicon batteries for EQE testing.

3 Results and discussion

3.1 Effect of surfactants

Figure 1(a) illustrates the perovskite film preparation process via blade printing of a perovskite precursor doped with surfactants. Figure 1(b) shows a large-area semitransparent perovskite film with an area of 5 cm × 5 cm produced via doctor-blading coating with a pinhole free, flat, and highly reflective surface. We demonstrate the planar photovoltaic device architecture of FTO\$TiO_2$\$CH(NH_2)_2PbBr_3$\Spiro-OMeTAD\Au (Fig. 1(c)) using $FAPbBr_3$ as an absorber layer, TiO_2 as an electron transport layer, and Spiro-OMeTAD as a hole transport layer.

An island-like perovskite morphology often appears in scalable printing processes. This non-ideal morphology may be related to the solution flow kinetics during the drying process of the perovskite solution [6]. At the beginning of the drying stage during coating, the perovskite and solvent react and generate micron-scale particles; these particles then begin to move and crystallize to form perovskite islands [11]. Under the influence of such a large-scale migration, it is challenging to fabricate uniform, pinhole-free perovskite films over large areas.

To suppress the solution flow to form more uniform perovskite films, we added amphiphilic surfactants to the perovskite precursor solution. Several types of surfactants were investigated to assist in the perovskite blade coating. The concentrations of the different surfactants added to the precursors were the same (0.2 mg/mL); these surfactants included l-α-phosphatidylcholine (LP), polyoxyethylene sorbitan monooleate (Tween), sodium laurylsulfonate (SLS), and hexadecyl trimethyl ammonium bromide (CTAB). Figure 2 shows SEM images of perovskite films with different surfactants. The control sample without a surfactant shows a discontinuous morphology,

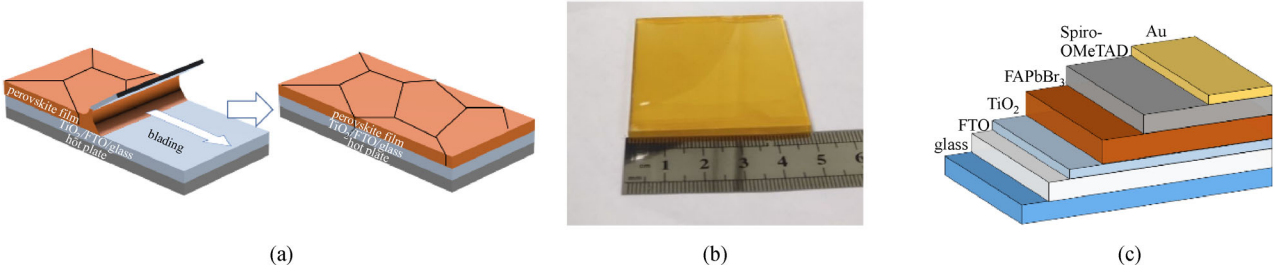

Fig. 1 (a) Descriptive illustration of the blade-coating process. (b) Large-area semitransparent perovskite film with an area of 5 cm × 5 cm. (c) Device structure of a doctor-bladed $FAPbBr_3$ solar cell

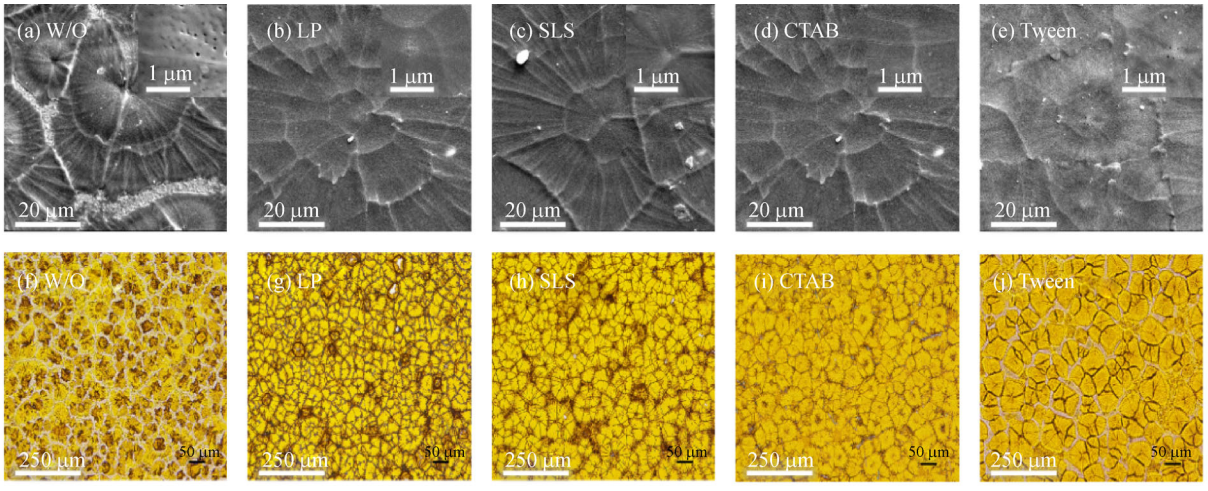

Fig. 2 SEM images of the $FAPbBr_3$ films fabricated via doctor blading (a) without surfactants and with (b) LP; (c) SLS; (d) CTAB; and (e) Tween surfactants. Optical microscopy images of the $FAPbBr_3$ films fabricated via doctor blading (f) without surfactants and with (g) LP; (h) SLS; (i) CTAB; and (j) Tween surfactants

with huge perovskite islands of approximately 10–50 μm observed in the perovskite film. This causes exposure of the TiO_2 film and the formation of an island-like perovskite film (Figs. 2(a) and 2(f)), which is not suitable for device fabrication. When a small amount of surfactant was added, the interface state of the solution system changes significantly. This is because the solution–air interface transforms into a hydrocarbon–air interface, which reduces the surface tension. From the images, we can see that all of the surfactants suppress the island structure to varying degrees. As opposed to the other samples, on the micron scale, the films formed with the addition of CTAB were uniform and pinhole free. Conversely, the films with the addition of LP/SLS/Tween presented a few holes in the surface of the grain, which may affect the optoelectronic properties of the films (Figs. 2(b)–2(e)). From the optical microscopy observations, we determined that the CTAB samples had the best morphology (Figs. 2(g)–2(j)). The color distribution of the optical microscopy images with CTAB was uniform compared to the films with LP/SLS. The dark areas at the edges of the grains were significantly reduced, implying that the surface of the film became smoother.

We fabricated solar devices with films using the addition of different surfactants. Figure 3(a) illustrates the *J*–*V* characteristics of different devices prepared via blade coating with different surfactants added to the perovskite precursor solution. The values of the statistical PCE, open circuit voltage (V_{oc}), short-circuit current density (J_{sc}), and fill factor (FF) for the different samples are shown in Figs. 3(c)–3(f). We can see that the improvement in the device performance primarily arises from the increase in V_{oc} when the surfactant is added; the detailed photovoltaic results are presented in Table 1. The best device, prepared with CTAB, exhibits a PCE of 6.90% with a V_{oc} of 1.159 V, a J_{sc} of 8.00 mA/cm^2, and an FF of 0.74. In contrast to devices prepared with other surfactants, all the photovoltaic parameters of the CTAB-doped devices improved, especially FF and V_{oc}. We see that the integrated J_{sc} values in the EQE spectra of the devices based on other surfactants were lower than those in the devices based on CTAB. In addition, the highest EQE value, approaching 80%, was obtained for a device based on CTAB doping.

3.2 Optimization of coating temperature

As opposed to other perovskite materials, $FAPbBr_3$ has an exceptionally superior phase stability at elevated temperatures compared to its iodine counterpart. Pure $FAPbBr_3$ becomes tetragonal at approximately 150 K and then cubic at temperatures greater than 275 K [24–26]. This indicates that, during the preparation of a perovskite film, the temperature change causes limited stability issues for the phase of the $FAPbBr_3$ perovskite. The annealing process plays a decisive role in the crystallization process of perovskite films and enables better grain sizes and fewer defects [27]. Accordingly, we studied the effect of the annealing temperature on the growth of the film and the performance of the $FAPbBr_3$ devices.

The main distinction between hot blading and conventional post-annealing is the presence of the solvent concentration in the film. During the hot-blading process, the annealing process is carried out simultaneously with solvent evaporation, which could yield large crystalline grains [28]. The SEM images in Fig. 4 demonstrate that the perovskite thin films produced with hot blading (150°C) were uniform, pinhole-free, and covered the entire substrate. When the annealing temperature was below 150°C (130°C/140°C), the perovskite grain size was approximately 20–30 μm, which was smaller than the grain size that annealing at a temperature of 150°C. The images also indicate that the grain boundary was reduced compared to the condition at 150°C. As the blading temperature increased, the grain size stopped increasing and many pinholes appeared at the surface. This may be because temperatures that are too high accelerate the decomposition of the perovskite films and the removal of the residue solvent from the film.

Figure 5(a) shows the UV–vis absorption spectrum of different perovskite films prepared via blade coating at different blading temperatures. We see that the preparation temperature does not change the bandgap of the perovskite material. Meanwhile, the curves indicate that the different temperatures had an obvious influence on the absorption properties of the films. The sample with a 150°C blading temperature represented the highest absorption of the samples. This may be related to the obvious increase in the grain size for the perovskite films at this temperature.

XRD was used to characterize the crystal structure of the doctor-bladed perovskite films at the various blading temperatures. The perovskite phases were very similar except for their crystallinity, as seen from the XRD patterns in Fig. 5(b). The XRD spectra of the thin films fabricated at different blading temperatures (130°C–180°C) all showed their strongest diffraction peaks at 14.83°, 21.10°, and 29.87°, representing the (001), (011), and (002) crystal planes, respectively, of perovskite films [9,29] with typical cubic crystal structures. When the blading temperature was less than 150°C, in the cases of 130°C and 140°C, the XRD spectra presented an obvious diffraction peak at 12.25°, corresponding to diffraction from $PbBr_2$ crystals [16]. Associating with the SEM images, we attributed the diffraction peak in the perovskite structure to the incomplete reaction of FABr and $PbBr_2$. As the blading temperature increased to 150°C, the diffraction peak at 12.25° disappeared. Meanwhile, the diffraction peaks at 14.83°, 21.10°, and 29.87° were further enhanced. This result shows that the crystallinity of a thin film can be improved at higher temperatures. When the temperature was further increased, there was a slight decrease in the XRD intensity. The reduction in the peak intensity may be caused by the higher blading temperature, which promotes

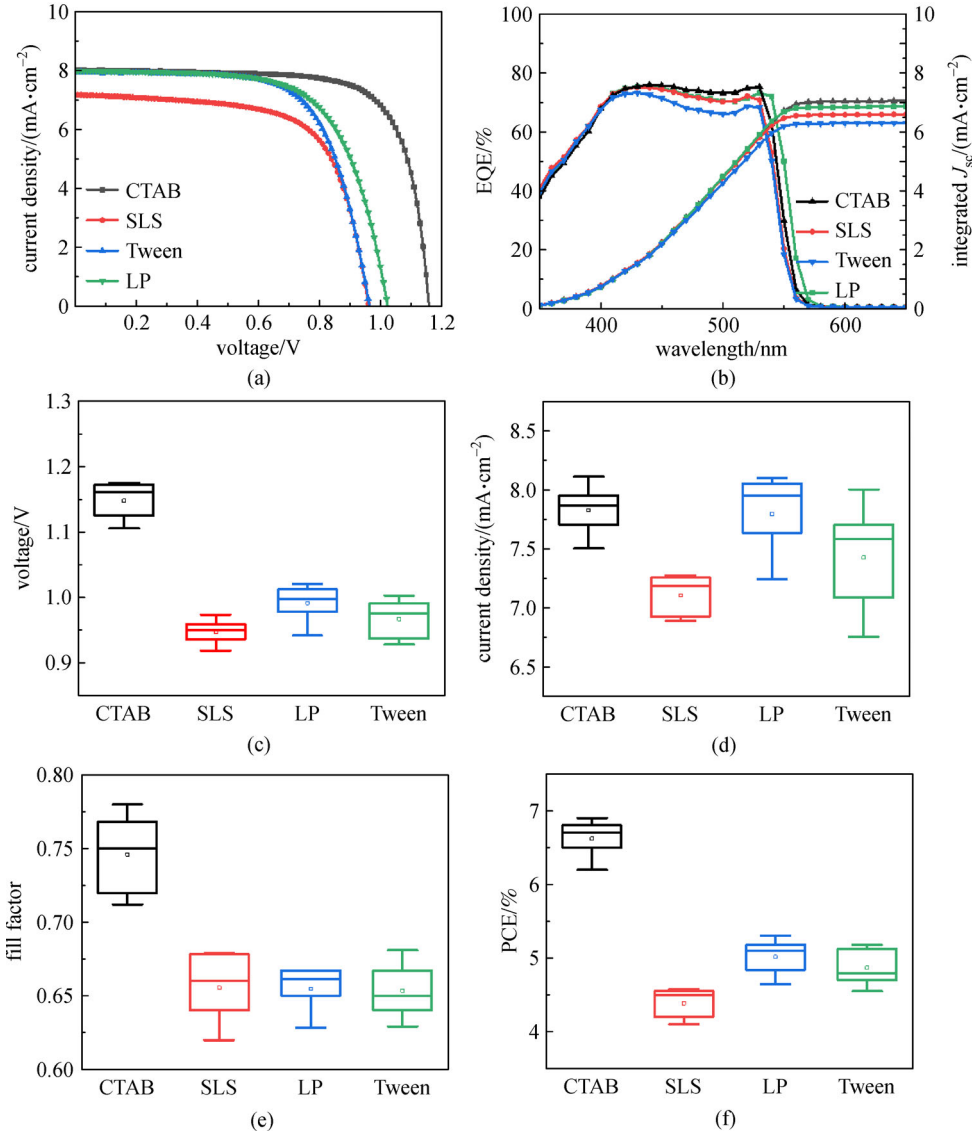

Fig. 3 (a) *J–V* curves of PSCs with different surfactants; (b) EQE spectra of the best devices prepared using different surfactants; and the effects of the addition of different surfactants on the statistical *J–V* parameters of the doctor-blading-printed devices: (c) J_{sc}; (d) V_{oc}; (e) FF; and (f) PCE

Table 1 Photovoltaic parameters of PSCs prepared using different surfactants

surfactant	V_{oc}/V	J_{sc}/(mA·cm^{-2})	FF	PCE/%
CTAB	1.159	8.00	0.74	6.90
SLS	0.961	7.17	0.66	4.58
Tween	0.964	7.92	0.68	5.19
LP	1.024	7.97	0.66	5.41

the evaporation of FABr and the incomplete reaction, in turn, results in the deterioration of the $FAPbBr_3$ film quality [6]. Therefore, a very high temperature does not present positive effects for the preparation of films. Taking the blading process into account, it is necessary to prepare high-quality $FAPbBr_3$ films at a suitable temperature.

The specific photovoltaic parameters of the different devices prepared at different temperatures are presented in Table 2. The average PCEs were 4.57% and 4.90% for samples processed at 130°C and 140°C, respectively. The PCEs were dramatically increased to 7.29% when the temperature increased to 150°C, with a V_{oc} of 1.175 V, a J_{sc}

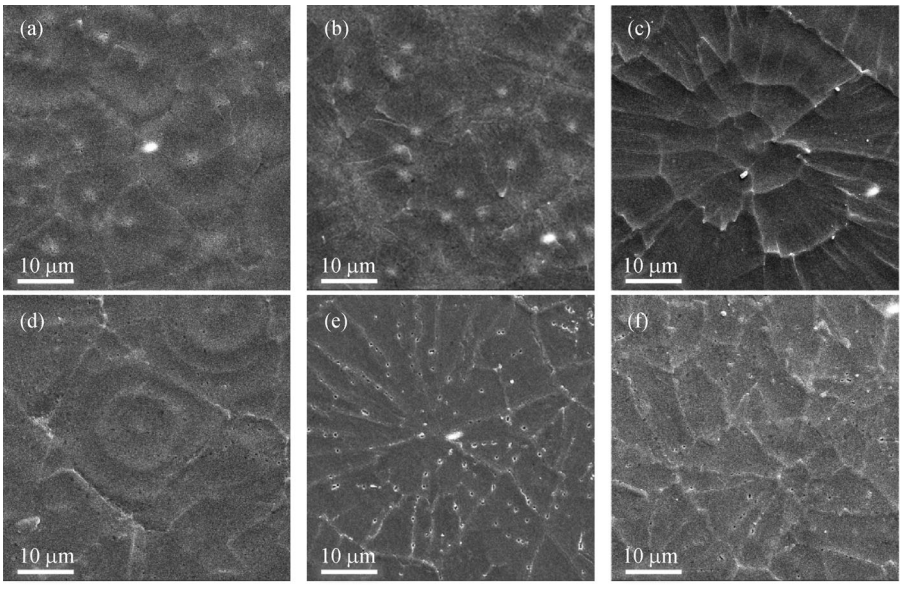

Fig. 4 SEM morphologies of perovskite films prepared at different annealing temperatures: (a) 130°C; (b) 140°C; (c) 150°C; (d) 160°C; (e) 170°C; and (f) 180°C

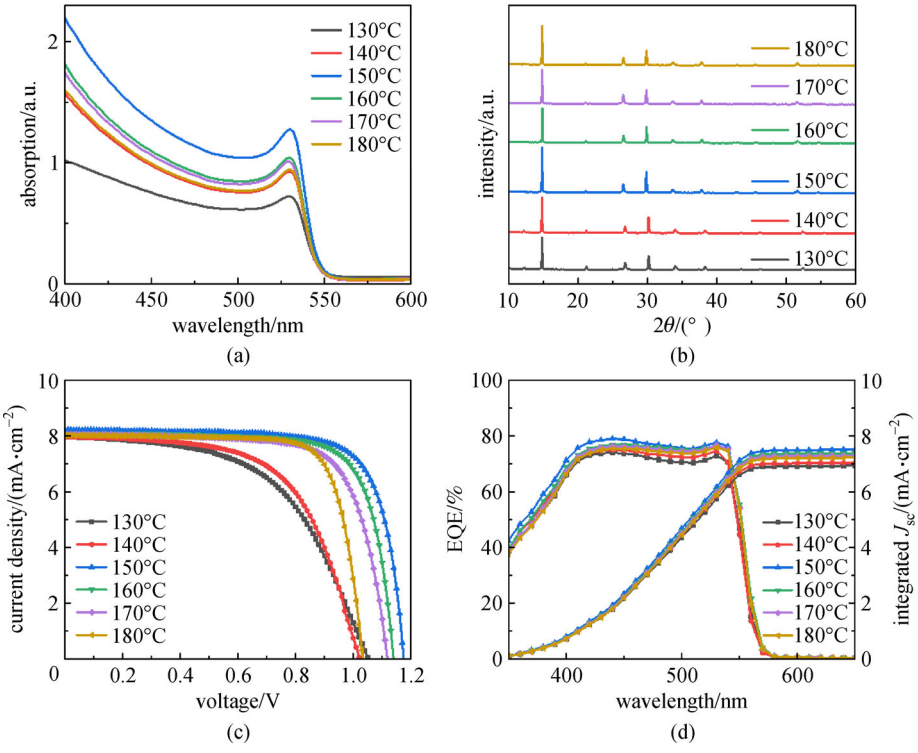

Fig. 5 Characterization of the devices prepared at various temperatures from 130°C to 180°C: (a) UV–vis absorption spectra; (b) X-ray diffraction; (c) *J–V* curves; and (d) EQE spectra of the best devices

of 8.22 mA/cm^2, and an FF of 0.75. Compared to the PSCs prepared at 130°C and 140°C, all the performance parameters were significantly improved. The *J–V* curves and EQE spectra of the PSCs are shown in Figs. 5(c) and 5(d), respectively. Further increasing the temperature to 160°C, 170°C, and 180°C, the PCEs decreased distinctly, primarily due to decreases in J_{sc} and V_{oc}. As discussed above, a high temperature results in the evaporation of

FABr, which can deteriorate the $FAPbBr_3$ phase and J_{sc} and V_{oc} accordingly. Therefore, we postulate that the optimum annealing temperature is 150°C.

However, the V_{oc} values of the prepared devices compared to the bandgap and reported studies are still very low. This may be because the coverage of the perovskite film fabricated via doctor blading still contains trance amounts of pinholes, which degrade V_{oc} [30,31]. The solvent extraction due to the heat treatment is not as efficient as the antisolvent route in spin coating. The energy band alignment may also need to be adjusted to allow efficient carrier transportation at the interface.

3.3 Preparation of semitransparent devices

Based on the above optimization of the blade coating of perovskite thin films, we fabricated ST-PSCs with silver nanowires; such devices are convenient and cost-effective for the preparation of semitransparent electrodes [32]. The structure of the perovskite semitransparent device was FTO\$TiO_2$\$FAPbBr_3$\Spiro-OMeTAD\AgNWs. The transmittance spectra are shown in Fig. 6(a); the average transmittance (AVT) (400–800 nm) of the FTO glass with a perovskite thin film was 50.83%. When a layer of Spiro-OMeTAD was deposited on top of the perovskite thin film via spin coating, the average transmittance (400–800 nm) was 51.18%. A Spiro-OMeTAD coating on a perovskite film can decrease the interface roughness [33], which enhances the transmittance of the device. We fabricated the transparent electrode by spray coating different volumes of AgNWs solutions using our reported method [2]. The average transmittance of ST-PSCs with 50 and 100 μL of AgNWs were 36.97% and 25.42%, respectively. Figure 6(b) shows the *J–V* characteristics of the ST-PSCs. When 50 μL of AgNWs was applied via spray coating, the average PCEs of the ST-PSCs were 4.61%. When the AgNWs volume increased to 100 μL, the average PCEs were clearly enhanced to 5.11%. The average photovoltaic parameters of the ST-PSCs are shown in Table 3. With increasing AgNWs, J_{sc} decreased slightly with enhanced V_{oc}. The ST-PSCs devices with and without AgNWs exhibit high transparency, as shown in Fig. 6(c).

Table 2 Photovoltaic parameters of blade-coated PSCs at different temperatures

Temperature/°C	V_{oc}/V	J_{sc}/(mA·cm^{-2})	FF	PCE/%
130	1.052	8.02	0.54	4.57
140	1.022	7.97	0.60	4.90
150	1.175	8.22	0.75	7.29
160	1.139	8.08	0.76	6.98
170	1.118	8.06	0.73	6.56
180	1.033	8.02	0.77	6.39

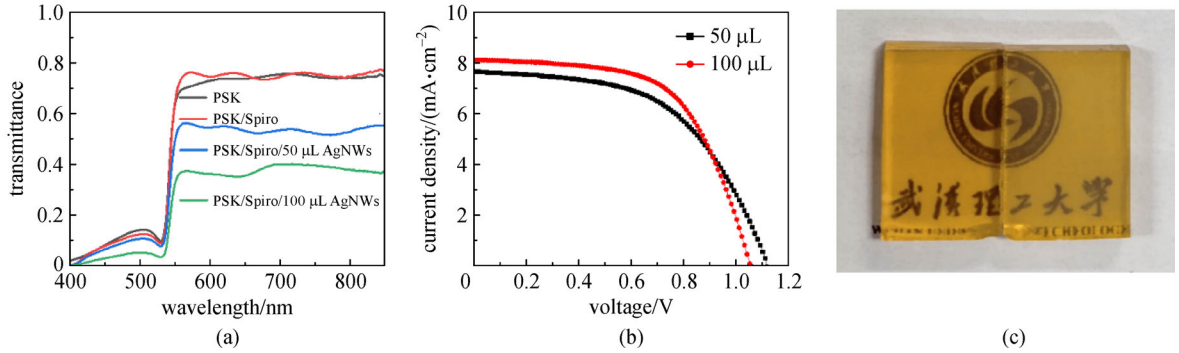

Fig. 6 (a) UV–vis transmittance spectra of samples with different stackings of the functional layers (PSK: perovskite); (b) *J–V* curves of the best devices prepared with different volumes of AgNWs; and (c) optical morphologies of devices without (left) and with (right) the transparent electrode

Table 3 Photovoltaic parameters of PSCs prepared with different volumes of AgNWs

volume/μL	V_{oc}/V	J_{sc}/(mA·cm^{-2})	FF	PCE/%
50	1.116	7.67	0.54	4.61
100	1.052	8.14	0.60	5.11

4 Conclusions

Uniform, pinhole-free $FAPbBr_3$ perovskite films were fabricated by adding surfactants to the precursor solution to improve the crystallization of the films via doctor-blade coating. In contrast to the precursor solution without an added surfactant, the addition of a surfactant effectively inhibited the production of defects and the resulting films had higher charge transfer efficiency and better uniformity. Therefore, during the large-area preparation process of perovskite, the surfactant CTAB can effectively improve the photoelectronic properties of $FAPbBr_3$ devices. PSCs prepared using this method exhibited on average a J_{sc} of 8.22 mA/cm^2, a V_{oc} of 1.175 V, and a PCE of 7.29%. The resulting semitransparent devices had a PCE of 5.11% and an AVT of 25.42%. This study therefore developed a doctor-blading process to fabricate wide-bandgap $FAPbBr_3$ films with the aim of producing high efficiency and semitransparent $FAPbBr_3$ solar cells.

Acknowledgements This work was financially supported by the National Key Research and Development Plan (No. 2017YFE0131900), the National Natural Science Foundation of China (Grant Nos. 51672202 and 21875178). J.Z. thanks the support from the "Chutian Scholar Program" of Hubei Province, China.

References

1. Jelle B P, Breivik C. State-of-the-art building integrated photovoltaics. Energy Procedia, 2012, 20: 68–77
2. Dou Y, Liu Z, Wu Z, Liu Y, Li J, Leng C, Fang D, Liang G, Xiao J, Li W, Wei X, Huang F, Cheng Y B, Zhong J. Self-augmented ion blocking of sandwiched 2D/1D/2D electrode for solution processed high efficiency semitransparent perovskite solar cell. Nano Energy, 2020, 71: 104567
3. Tai Q, Yan F. Emerging semitransparent solar cells: materials and device design. Advanced Materials, 2017, 29(34): 1700192
4. Bu T, Li J, Zheng F, Chen W, Wen X, Ku Z, Peng Y, Zhong J, Cheng Y B, Huang F. Universal passivation strategy to slot-die printed SnO_2 for hysteresis-free efficient flexible perovskite solar module. Nature Communications, 2018, 9(1): 4609
5. Bu T, Liu X, Zhou Y, Yi J, Huang X, Luo L, Xiao J, Ku Z, Peng Y, Huang F, Cheng Y B, Zhong J. A novel quadruple-cation absorber for universal hysteresis elimination for high efficiency and stable perovskite solar cells. Energy & Environmental Science, 2017, 10 (12): 2509–2515
6. Yang W S, Park B W, Jung E H, Jeon N J, Kim Y C, Lee D U, Shin S S, Seo J, Kim E K, Noh J H, Seok S I. Iodide management in formamidinium-lead-halide-based perovskite layers for efficient solar cells. Science, 2017, 356(6345): 1376–1379
7. Bu T, Wu L, Liu X, Yang X, Zhou P, Yu X, Qin T, Shi J, Wang S, Li S, Ku Z, Peng Y, Huang F, Meng Q, Cheng Y B, Zhong J. Synergic interface optimization with green solvent engineering in mixed perovskite solar cells. Advanced Energy Materials, 2017, 7(20): 1700576
8. NREL Chart. Best research-cell efficiencies. 2020
9. Zhang Y, Liang Y, Wang Y, Guo F, Sun L, Xu D. Planar $FAPbBr_3$ solar cells with power conversion efficiency above 10%. ACS Energy Letters, 2018, 3(8): 1808–1814
10. Barrows A T, Pearson A J, Kwak C K, Dunbar A D F, Buckley A R, Lidzey D G. Efficient planar heterojunction mixed-halide perovskite solar cells deposited via spray-deposition. Energy & Environmental Science, 2014, 7(9): 2944–2950
11. Ye F, Chen H, Xie F, Tang W, Yin M, He J, Bi E, Wang Y, Yang X, Han L. Soft-cover deposition of scaling-up uniform perovskite thin films for high cost-performance solar cells. Energy & Environmental Science, 2016, 9(7): 2295–2301
12. Kim J H, Williams S T, Cho N, Chueh C C, Jen A K Y. Enhanced environmental stability of planar heterojunction perovskite solar cells based on blade-coating. Advanced Energy Materials, 2015, 5 (4): 1401229
13. Deng Y, Dong Q, Bi C, Yuan Y, Huang J. Air-stable, efficient mixed-cation perovskite solar cells with Cu electrode by scalable fabrication of active Layer. Advanced Energy Materials, 2016, 6 (11): 1600372
14. Yang M, Li Z, Reese M O, Reid O G, Kim D H, Siol S, Klein T R, Yan Y, Berry J J, van Hest M F A M, Zhu K. Perovskite ink with wide processing window for scalable high-efficiency solar cells. Nature Energy, 2017, 2(5): 17038
15. Deng Y, Zheng X, Bai Y, Wang Q, Zhao J, Huang J. Surfactant-controlled ink drying enables high-speed deposition of perovskite films for efficient photovoltaic modules. Nature Energy, 2018, 3(7): 560–566
16. Hwang K, Jung Y S, Heo Y J, Scholes F H, Watkins S E, Subbiah J, Jones D J, Kim D Y, Vak D. Toward large scale roll-to-roll production of fully printed perovskite solar cells. Advanced Materials, 2015, 27(7): 1241–1247
17. Wang D, Zheng J, Wang X, Gao J, Kong W, Cheng C, Xu B. Improvement on the performance of perovskite solar cells by doctor-blade coating under ambient condition with hole-transporting material optimization. Journal of Energy Chemistry, 2019, 38(1): 207–213
18. Deng Y, Peng E, Shao Y, Xiao Z, Dong Q, Huang J. Scalable fabrication of efficient organolead trihalide perovskite solar cells with doctor-bladed active layers. Energy & Environmental Science, 2015, 8(5): 1544–1550
19. He M, Li B, Cui X, Jiang B, He Y, Chen Y, O'Neil D, Szymanski P, Ei-Sayed M A, Huang J, Lin Z. Meniscus-assisted solution printing of large-grained perovskite films for high-efficiency solar cells. Nature Communications, 2017, 8(1): 16045
20. Tang S, Deng Y, Zheng X, Bai Y, Fang Y, Dong Q, Wei H, Huang J. Composition engineering in doctor-blading of perovskite solar cells. Advanced Energy Materials, 2017, 7(18): 1700302
21. Ye F, Tang W, Xie F, Yin M, He J, Wang Y, Chen H, Qiang Y, Yang X, Han L. Low-temperature soft-cover deposition of uniform large-scale perovskite films for high-performance solar cells. Advanced Materials, 2017, 29(35): 1701440
22. Zuo L, Shi X, Fu W, Jen A K. Highly efficient semitransparent solar cells with selective absorption and tandem architecture. Advanced Materials, 2019, 31(36): 1901683
23. Liu X, Bu T, Li J, He J, Li T, Zhang J, Li W, Ku Z, Peng Y, Huang F, Cheng Y B, Zhong J. Stacking n-type layers: effective route

towards stable, efficient and hysteresis-free planar perovskite solar cells. Nano Energy, 2018, 44: 34–42
24. Dai J, Zheng H, Zhu C, Lu J, Xu C. Comparative investigation on temperature-dependent photoluminescence of $CH_3NH_3PbBr_3$ and $CH(NH2)_2PbBr_3$ microstructures. Journal of Materials Chemistry C, Materials for Optical and Electronic Devices, 2016, 4(20): 4408–4413
25. Wright A D, Verdi C, Milot R L, Eperon G E, Pérez-Osorio M A, Snaith H J, Giustino F, Johnston M B, Herz L M. Electron-phonon coupling in hybrid lead halide perovskites. Nature Communications, 2016, 7(1): 11755
26. Galkowski K, Mitioglu A A, Surrente A, Yang Z, Maude D K, Kossacki P, Eperon G E, Wang J T, Snaith H J, Plochocka P, Nicholas R J. Spatially resolved studies of the phases and morphology of methylammonium and formamidinium lead trihalide perovskites. Nanoscale, 2017, 9(9): 3222–3230
27. Bi C, Shao Y, Yuan Y, Xiao Z, Wang C, Gao Y, Huang J. Understanding the formation and evolution of interdiffusion grown organolead halide perovskite thin films by thermal annealing. Journal of Materials Chemistry A, Materials for Energy and Sustainability, 2014, 2(43): 18508–18514
28. Nie W, Tsai H, Asadpour R, Blancon J C, Neukirch A J, Gupta G, Crochet J J, Chhowalla M, Tretiak S, Alam M A, Wang H L, Mohite A D. High-efficiency solution-processed perovskite solar cells with millimeter-scale grains. Science, 2015, 347(6221): 522–525
29. Hanusch F C, Wiesenmayer E, Mankel E, Binek A, Angloher P, Fraunhofer C, Giesbrecht N, Feckl J M, Jaegermann W, Johrendt D, Bein T, Docampo P. Efficient planar heterojunction perovskite solar cells based on formamidinium lead bromide. Journal of Physical Chemistry Letters, 2014, 5(16): 2791–2795
30. Gao L, Yang G. Organic-inorganic halide perovskites: from crystallization of polycrystalline films to solar cell applications. Solar RRL, 2020, 4(2): 1900200
31. Li Y, Ding B, Chu Q Q, Yang G J, Wang M, Li C X, Li C J. Ultra-high open-circuit voltage of perovskite solar cells induced by nucleation thermodynamics on rough substrates. Scientific Reports, 2017, 7(1): 46141
32. Yang K, Li F, Zhang J, Veeramalai C P, Guo T. All-solution processed semi-transparent perovskite solar cells with silver nanowires electrode. Nanotechnology, 2016, 27(9): 095202
33. Kim H, Kim H S, Ha J, Park N G, Yoo S. Empowering semi-transparent solar cells with thermal-mirror functionality. Advanced Energy Materials, 2016, 6(14): 1502466

Hangkai Ying is currently undertaking his Master's degree in State Key Lab of Advanced Technology for Materials Synthesis and Processing, Wuhan University of Technology, China. His research interests focus on the wide-gap perovskite solar cells and doctor-blade coating.

Yifan Liu is currently undertaking his Master's degree in State Key Lab of Advanced Technology for Materials Synthesis and Processing, Wuhan University of Technology, China. His research interests focus on developing novel and stable perovskite solar cells.

Yuxi Dou is currently undertaking his Master's degree in State Key Lab of Advanced Technology for Materials Synthesis and Processing, Wuhan University of Technology, China. His research interests focus on the transparent electrode and semitransparent perovskite solar cells.

Jibo Zhang is currently undertaking his Master's degree in State Key Lab of Advanced Technology for Materials Synthesis and Processing, Wuhan University of Technology, China. His research interests focus on the superhydrophobic encapsulated films.

Zhengli Wu is currently undertaking his Master's degree in State Key Lab of Advanced Technology for Materials Synthesis and Processing, Wuhan University of Technology, China. His research interests focus on the doping and interface control of perovskite solar cells.

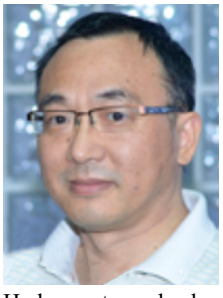

Qi Zhang received his B.Sc. degree in Electrochemistry, M.Sc. degree in Inorganic Materials and Ph.D. degree in Sol-Gel Chemistry. He joined Cranfield University, UK as a Research Fellow in 1996 following the completion of a Ph.D. degree at Monash University in Australia. He became a Senior Research Fellow in 1998, and then Senior Lecturer in 2007. He has a strong background in ferroelectric thin and thick films and their applications in ferroelectric mempry, pyroelectric and electrocaloric effect; in the synthesis of nanofunctional materials and their applications in ink-jet printing, and surface modifications; and in nanomaterials for energy storage, etc.

Yi-Bing Cheng is a professor in Department of Materials Engineering at Monash University, Australia. He completed his undergraduate (1978) and Master (1983) studies at Wuhan University of Technology, China and received a Ph.D. degree from University of Newcastle-upon-Tyne, UK in 1989. He specializes in inorganic materials and composites. He started working on dye sensitized solar cells in 2001 and is mainly interested in solution processed solar cells.

Jie Zhong received his Ph.D. degree in December 2011 from Central South University, China. He was studied in Department of Engineering, Monash University, Australia as a visiting student and work on sol-gel processed ceramics, supervised by Prof. Yi-Bing Cheng. In 2015, he joined State Key Lab of Advanced Technology for Materials Synthesis and Processing, Wuhan University of Technology, China as associate professor and was awarded as the “Chutian Scholar” of Hubei province in 2016. His current research interests focus on solution processed optoelectronics and functional coatings for energy and environmental applications.